VALIDATION OF AREVA's BEST PRACTICES IN THE EPRI ROUND ROBIN BENCHMARK

M. Martin*, T. Keheley
AREVA Inc.
2101 Horn Rapids Road, Richland WA 99352, USA
Mathieu.Martin@areva.com; Thomas.Keheley@areva.com

K. Vogel, K. Goodheart
AREVA GmbH
Paul-Gossen-Str. 100, 91052 Erlangen Germany
Klaus.Vogel@areva.com; Kevin.Goodheart@areva.com

A. Hatman
AREVA Inc.
3315 Old Forest Road, Lynchburg VA 24501, USA
Anca.Hatman@areva.com

A. Chatelain
AREVA NP
10 rue Juliette Récamier, 69456 Lyon, France
Alexandre.Chatelain@areva.com

ABSTRACT

Accurate predictions of local thermal-hydraulics condition are crucial for the success of a level IV CIPS/CILC assessment. Carried out in the framework of Crud-Induced Power Shift risk assessment analyses in PWR cores, the CEA-EDF-EPRI collaborative NESTOR project aimed to produce accurate thermal-hydraulic experimental data on 5×5 rod bundles. The NESTOR project has obtained high fidelity thermal hydraulic data in prototypic conditions. The dataset includes single-phase (heated and adiabatic) pressure drop, flow field (axial velocity), wall temperature and thermal-mixing data through experiments performed at CEA in the MANIVEL and OMEGA loops.
The EPRI round robin CFD benchmark exercise consists of two phases, structured based on the rod bundle grid configurations: simple support grids and mixing vane grids. It allowed participants to benchmark their CFD codes and methodologies against the NESTOR dataset.
AREVA had already developed and presented its methodology in previous publications but the participation to the round robin CFD benchmark, provides the opportunity to benchmark the existing CFD "best-practices" against this comprehensive high fidelity dataset. Using the CFD code STAR-CCM+®[1], by CD-adapco™, it was possible to get very good agreement between predictions and experimental measurements. Over the course of the benchmark, it was possible to tune and learn the effect of different modeling approaches to get best agreement with the test data. For example, conjugate heat transfer and volumetric heat source in the cladding proved to be very important in order to accurately predict wall

* Corresponding authors
[1] CD-adapco™ and STAR-CCM+® are registered trademarks or trademarks of CD-adapco in the USA or other countries.

temperature. Also, the impact of the turbulence modeling showed to be crucial for accurate predictions of both simple support grid and mixing vane spacer grid.

KEYWORDS
CFD; CRUD; fuel bundle; PWR

1. INTRODUCTION

The Round Robin (RR) EPRI benchmark used high fidelity test data collected during the collaborative CEA-EDF-EPRI NESTOR project. The NESTOR project [1] aimed at providing data to help evaluate two major concerns for Pressurized Water Reactor (PWR) operation: Crud-Induced Local Corrosion (CILC) and Crud-Induced Power Shift (CIPS). Both result from localized accumulation of corrosion products at the surface of the rods. Ultimately these can lead to fuel failure. Because of the localized nature of the Crud deposition, Computational Fluid Dynamics (CFD) is the only tool to accurately evaluate and predict Crud related problems. The Electric Power Research Institute (EPRI) recommends this level of analysis in the "Level IV Evaluation Methods" where CFD is used to accurately model the realistic Thermal Hydraulic (TH) conditions to predict risk associate with Crud in a rod bundle.
CFD needs to be benchmarked against high fidelity test data to ensure that the models are capable of representing accurately the TH behavior inside a fuel assembly. This is the motivation of the NESTOR project and the EPRI RR benchmark. Using the high fidelity data collected during the NESTOR project, the participants are given the opportunity to benchmark their CFD methods.
Crucial data for thermal hydraulic bundle data (pressure drop, flow field, wall temperature and thermal mixing) were collected under prototypic conditions. The first campaign used only simple support grids (SSG) in the bundle. Typically light water reactor fuel assemblies include structural grids to maintain the rod array shape. Along the years this structural elements were modified and optimized to improve thermal hydraulic performances: pressure drop, thermal mixing and overall performance. SSGs are purely structural grids and barely affect the flow. They are typically used for testing. The second campaign included an actual prototypic Mixing Vane Grid (MVG). This MVG is consistent with an actual grid used in reactor. It includes vanes used to condition the flow and improve the TH performance of the bundle.
An extensive set of quality data was collected by CEA/EDF in the MANIVEL and OMEGA loops. MANIVEL provided adiabatic measurements of a 5x5 full length bundle and OMEGA provided data under PWR conditions including rod wall temperatures, and temperature of the fluid at the center of the subchannels. This testing using prototypic hardware and providing heated bundle measurement under reactor conditions provides relevant benchmark data for CFD. Reference [2] presents an overview of the RR benchmark.

Throughout the course of this benchmark, all participants were given the opportunity to compare their methods and benchmark them against this dataset. AREVA has been using CFD as a design and assessment tool for its fuel for over 15 years. Very extensive validations have been performed against in-house collected data. Best practices and guidelines are in place to ensure quality and accuracy. These methods have already been used for Level IV Crud assessment [3]. As part of the RR benchmark, AREVA had the opportunity to benchmark its CFD methodology against this extensive dataset.
This paper presents a summary of the results obtained and some discussion around the different methods used. The paper will follow the structure of the benchmark. First the results associated with the MANIVEL experiments will be detailed, and then the results associated with the heated bundle, based on the OMEGA experiments, part of the benchmark. Relevant information about the test will be provided to help understand and justify the CFD modeling.

2. ISOTHERMAL CASE: MANIVEL

2.1. Test description

The NESTOR-MANIVEL isothermal experiment gathered data from adiabatic rod bundle tests. A full length 5x5 rod array was used. The casing was instrumented to measure pressure drop around the MVGs. The test section was also equipped to be able to measure flow fields using Laser-Doppler Velocimetry (LDV). Two-dimensional mean and RMS values of local axial velocity distribution over several axial cross sections were extracted. The NESTOR-MANIVEL test loop operates at atmospheric condition. The flow rate is 64.7 m^3/h and the temperature 29.7 degrees C. The test section contains SSGs and MVGs. Note that the MVGs are rotated 90 degrees at each elevation compared to the previous. A SSG is present between each MVG.

2.2. CFD modeling

A CFD model is built to represent the section of the measurements. Two MVGs and 3 SSGs are included (see Figure 1). Since this test is isothermal, periodic boundary conditions can be used to simulate an infinite bundle. AREVA has developed best practices to compute pressure drops and flow field from fuel assembly [4]. The same parameters for meshing and physics are used. Note that the geometry and all the hardware are explicitly modeled from the provided Computer Aided Design (CAD) models of the MVG and the SSG. The use of periodic boundaries is justified since the outlet conditions are the same as the inlet of the domain. The measurement section starts downstream the first spacer, in the bundle this spacer is located downstream an SSG which justifies the applied conditions from the outlet of the domain. Lengths are adjusted so the rod length between the last SSG and the first MVG are consistent with the real bundle. The impact of the vane spacer over the flow is expected to overcome any prior flow features. The model could have probably been further reduced while still maintaining the main flow characteristics.

CD-adapco™ STAR-CCM+® version 8.06 [5] was used in this work.
Figure 2 shows the mesh at different axial locations (inside the MVG, in the rod bundle and inside the SSG). A trim mesh is used made mostly of hexahedral cells. The base size is 0.3mm. The surface mesh is refined on the SSGs and MVGs to properly capture the steep gradients caused by the hardware. Two prism layers are applied against the rods to properly model the effect of the wall friction on the flow. The first layer is sized to guarantee that the Y+ value is around 65 in the majority of the domain. The entire CFD model contained ~112 million cells.

In the NESTOR-MANIVEL portion of the benchmark, single-phase adiabatic flow characteristics are considered. The presence of the spacer grids induce significant amount of turbulence that needs to be appropriately modeled. AREVA's methodology uses a modified k-epsilon quadratic formulation [6] that is specifically tuned to model the turbulence inside a rod bundle. Rod friction is also a major contributor to the pressure drop and the behavior of the flow field. The high Y+ wall function is used to resolve the boundary layer. This model requires the Y+ value to be maintained higher than 35. The Segregated solver of STAR-CCM+® is used. The simulation is single-phase, and assumes steady state flow, as no strong time dependent fluctuations are expected.

Figure 1: MANIVEL CFD geometry

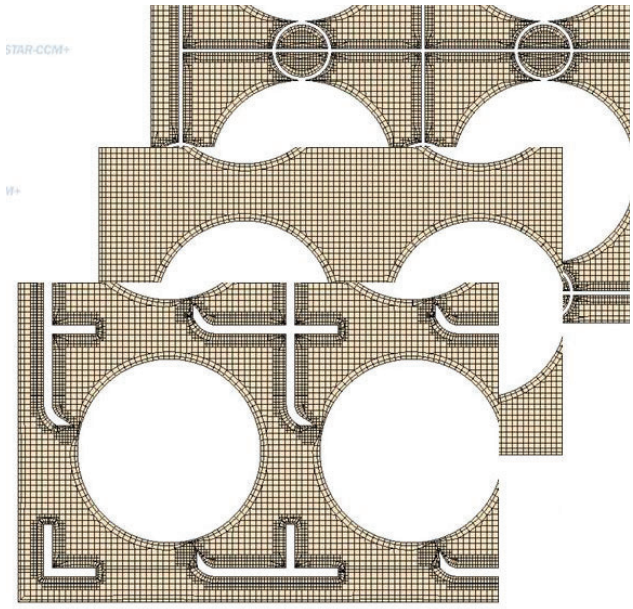

Figure 2: MANIVEL CFD mesh

2.3. Pressure drop

The pressure drop was measured between each element. AREVA's existing best practices have shown good agreement, within the test measurements uncertainty, for single-phase pressure drop prediction with CFD. The average deviation between predicted and measured pressure drop is typically on the order of ±3%. The data are extracted around each spacer and the agreement is 1.7% and 2.62% respectively for spacer IDs 131 and 127 in Figure 3. The SSG exhibits a difference of 15.9% between CFD and measurements. In this particular case, the friction of the rods is the major contributor as the SSG has a very weak effect on the flow however the expected agreement of the measurements across the spacer grid shows a good behavior leading to question the accuracy of this measurement. Some secondary effects, not properly captured by the CFD model can become predominant in the case of the SSG (flow area, geometric discrepancies between ideal CAD and tested geometry...).

2.4. Flow field

Another element of the single phase isothermal case was the flow field data using LDV measurements. Figure 5 through Figure 9 show the comparisons in the axial velocity between CFD and measurements. Several axial locations are shown downstream of the spacer grid and the SSG. Figure 3 presents the axial location relative to each element. In this paper, only one location is illustrated y=0.0266m (see Figure 4). This location is chosen since it should be further from the walls and therefore more meaningful with respect to the impact of the MVG over the flow.

The measurements and the CFD predictions are plotted together for the axial velocity at different elevations. Figure 5 through Figure 9 show the comparison for different axial elevations. Figure 5 shows the axial velocity value 2.5cm downstream of the spacer. The axial velocity is quite disturbed due to the proximity of the spacer and its strong residual effect. CFD manages to capture the major peaks, both their amplitude and location. One also needs to consider that the uncertainty, reported to be about ± 1.5% for

the measurements, might be increased due to the proximity of the MVG and the very disturbed flow. As the measurements gets further downstream, the effect of the MVG disappears and the difference between peak and average is less obvious. Measurements probably also suffer from the lack of gradients. Figure 6 and Figure 7 show these elevations where the structure of the flow is not as well defined; there is no dominating effect between the dying effect of the MVG and the relatively growing impact of the rod friction. Further downstream, Figure 8 shows the axial velocity downstream the SSG. The structure of the flow becomes more defined again; the friction of the rod becomes more dominant since the SSG does not introduce much flow disturbance. One can notice the residual impact of the strips in the middle of the subchannels. Further downstream, Figure 9 shows the undisturbed flow. The effect of the SSG is no longer present, only the friction is governing the lateral gradients. The subchannels are well defined, with the peak of velocity at the center.

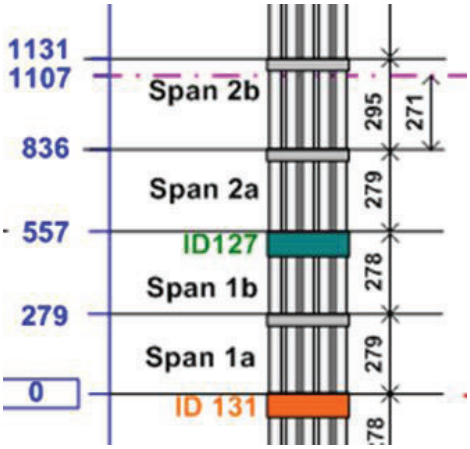

Figure 3: Axial location distribution of the bundle

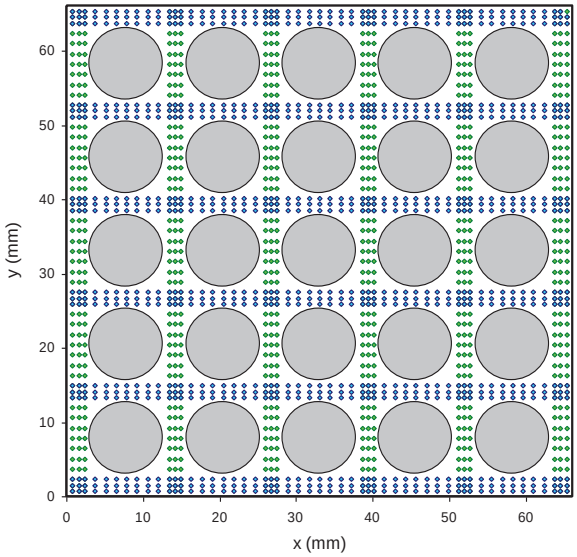

Figure 4: LDV configuration

CFD predicts well the axial flow features. The high disturbance regions, directly downstream of the MVG is still challenging to accurately predict but the measurements are also probably affected. The peaks and overall amplitudes are also well predicted. A good agreement is achieved both quantitatively and qualitatively between test and CFD predictions.

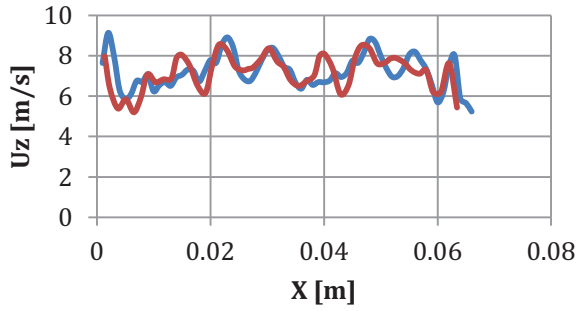

Figure 5: Axial velocity at z= 0.025m

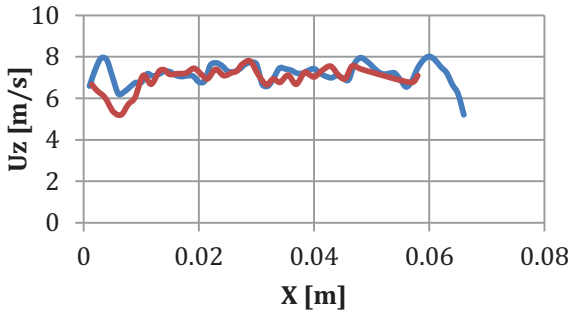

Figure 6: Axial velocity at z= 0.05m

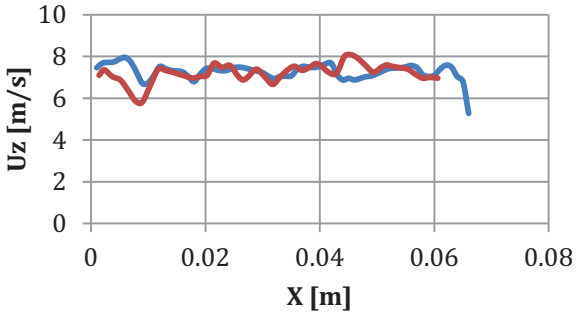

Figure 7: Axial velocity at z= 0.075m

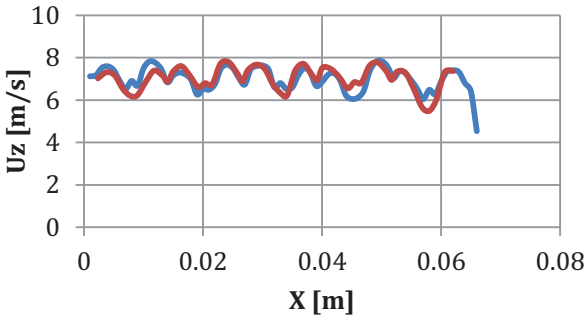

Figure 8: Axial velocity at z= 0.304m

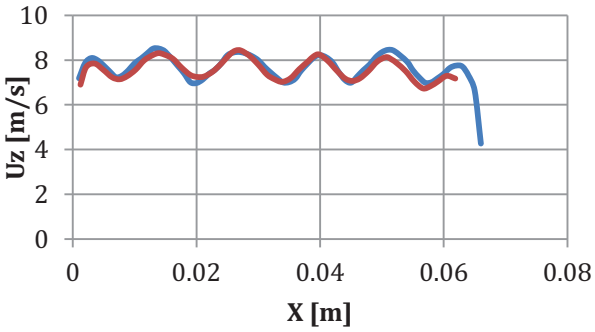

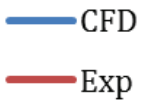

Figure 9: Axial velocity at z= 0.514m

3. HEATED BUNDLE CASE: OMEGA

The second set of data used for this Round Robin EPRI benchmark was taken from a heated bundle experiment performed at CEA Grenoble in the OMEGA loop. A 5x5 rod bundle including SSGs and MVGs was tested using heater rods. Wall temperature measurements were taken using innovative techniques [1-2], allowing accurate measurements inside the cladding of each rod, offering both an axial and azimuthal temperature distribution.

The challenge for CFD was to build a model representative of this very complex experiment. Obviously, the hardware needs to be explicitly modeled to properly capture the effect on the flow. The entire heated length was modeled using the full 5x5 array. This was required to get the accurate temperature distribution at the measurement locations. The test used direct heater rods, which means that the heat is

generated in the cladding by applying an electrical current. The resistance of the cladding governs the heating of each rod. Two sets of rods were used. The center 3x3 called “hot rods” used a higher heating power than the peripheral rows called “cold rods”.

3.1. CFD modeling

The region of interest where the data were taken includes the last 3 spans before the End Of Heated Length (EOHL); therefore everything upstream has little direct impact on the solution except for adequately conditioning the flow and temperature distributions. For accuracy and automation purposes the entire geometry was modeled with the same mesh resolution. A mass flux was applied at the inlet of the domain consistent with the test inlet conditions.

To adequately model the wall heat flux, the cladding was modeled and meshed. Conjugate heat transfer was used to solve for the heat conduction inside the cladding and the heat transfer into the fluid. The power was applied as a power density calculated from the power applied during the test. This allows a strong coupling between the surface heat flux generation and the local fluid temperature outside the cladding. As opposed to traditional surface heat flux applied on the outside of the cladding which applies a constant surface heat flux value regardless of local condition (eg, impingement of colder water on the rod). Considering the cladding is a major condition to properly model a heated bundle and get an accurate wall temperature. An adiabatic boundary condition was applied inside the cladding.

STAR-CCM+® version 8.06 was used [5]. A trim mesh (mostly hexahedral cells) was built in the fluid domain. The base size of the cell is 0.45mm to save on the overall number of cells. The entire domain is built by adding different elements (MVGs, SSGs) and the rod sections are created by extruding the axial faces of each element. A 0.6mm axial extrusion is applied. The resolution near the heated walls is crucial in order to properly capture the temperature distribution and the heat transfer between solid and liquid. It was found that 4 prism layers give adequate results. The first layer is set so that the Y+ value is consistently between 65 and 95 to be consistent with the wall functions and the turbulence model.
The cladding is meshed separately using STAR-CCM+ ® “thin mesher” which allows building layers of polyhedral cells throughout the thickness of the cladding. It was found that layers of 0.15mm give a good representation of the conduction inside the cladding. Figure 10 illustrates the volume mesh used for both the solid and the fluid domains. Note that the two meshes are not perfectly conformal, therefore some interpolation is performed between fluid and solid through an interface. The overall mesh, including 6 MVGs, 7 SSGs and the full 5x5 array totaled 220 million cells in the fluid domain and 23 million in the cladding.

STAR-CCM+ ®, segregated solver was used to calculate the solution. A Steady state, single phase calculation using the modified k-epsilon quadratic model [6] was performed. Three-dimensional conduction was solved inside the cladding. Water properties were applied as tables to represent the different properties under the range of temperature encountered.

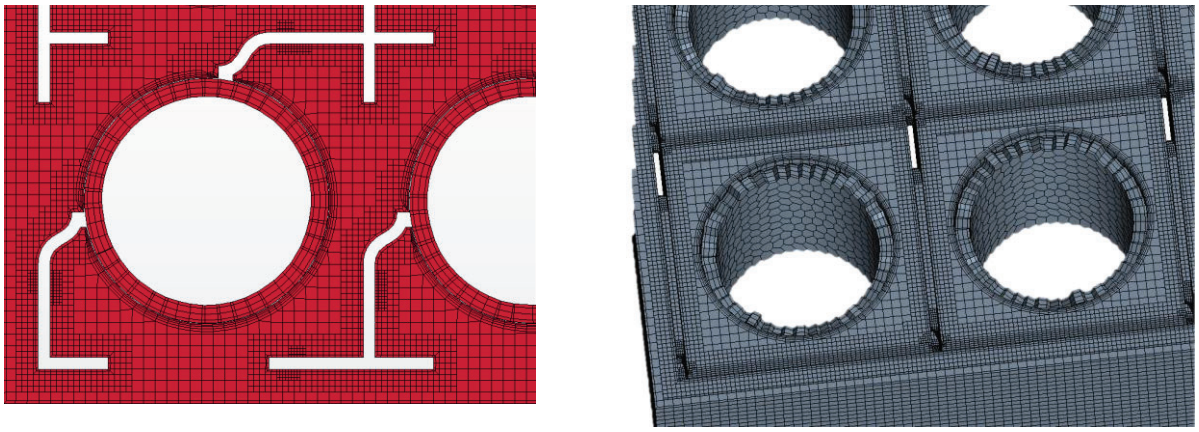

Figure 10: Volume mesh

3.2. Sensitivity studies

The high quality of the experiments and the data collected allowed performing some sensitivity analyses to determine the best modeling technique. At an industry level, some limitations need to be considered: computer power available and time to reach a stable solution. Some sacrifices have to be made in order to efficiently and accurately obtain a solution. This balance between resources and accuracy has to be evaluated through several parameters like the mesh resolution, or the physical models used. During this benchmark some sensitivity studies were performed to quantify and evaluate the impact of the some of these choices. The main conclusions are detailed.

Two meshes were generated using target cell sizes of 0.45mm and 0.3mm respectively. For the heated bundle case, the cell size was increased to 0.45mm to save on the total number of cells since the entire heated length needed to be represented. Figure 11 illustrates the difference between both meshes. Other parameters were maintained the same. The traditional modified k-epsilon quadratic turbulence model was also compared against the default k-epsilon Realizable in STAR-CCM+®.

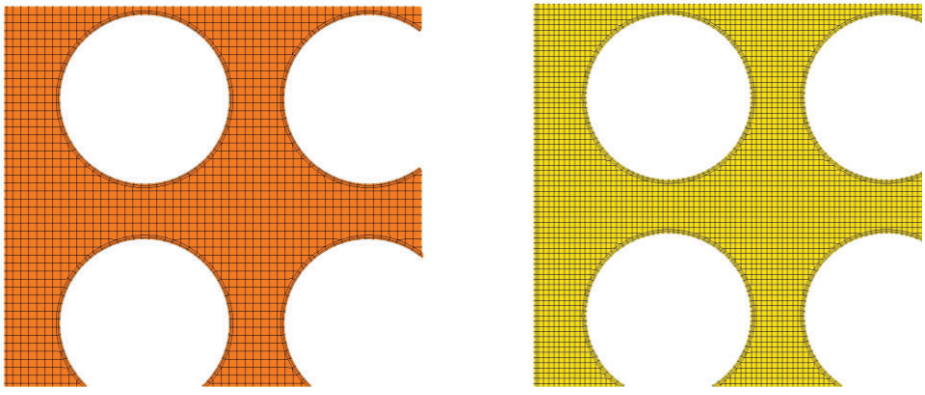

Figure 11: left, 0.45mm mesh; right, 0.3mm mesh

To illustrate the differences, between meshes and turbulence models, Figure 12 shows a comparison between each model to predict inner-wall temperature against experiment throughout an entire span at one

angular location for Rod 1. The modified k-epsilon quadratic seems to capture better the overall trend of the temperature distribution. The peaks are more in phase downstream of the MVG (even if they are slightly over predicted) with the measurements. The overall trend, especially downstream the SSG is more consistent with the measurement. Both meshes are also compared and do not show significant differences.

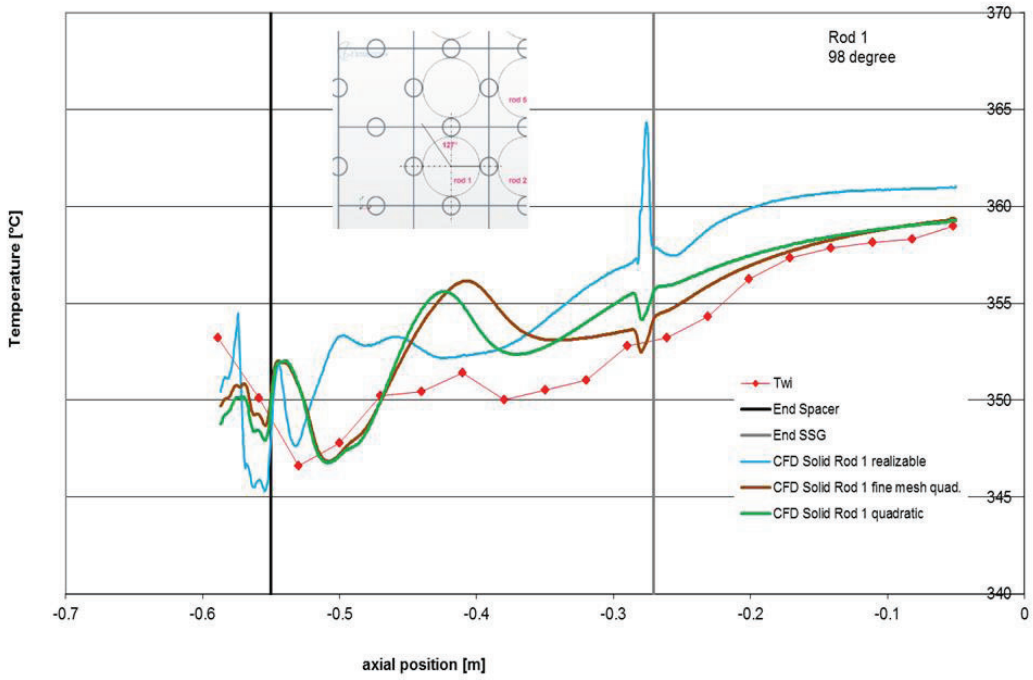

Figure 12: Axial inner-wall temperature distribution for Rod 1 at 98 degrees.

Figure 13 compares the same parameters on circumferential temperature distribution around Rod 1 at two elevations (-0.111 and -0.5m) respectively downstream of the last SSG and of the last MVG. Downstream of the SSG, as expected the wall temperature is fairly uniform. The trend is well predicted by the modified k-epsilon quadratic. Downstream of the MVG, where the gradients are stronger, both turbulence models give virtually the same results. As was described previously the peak is over-predicted compared to the experiment. The different meshes do not seem to have a significant impact.

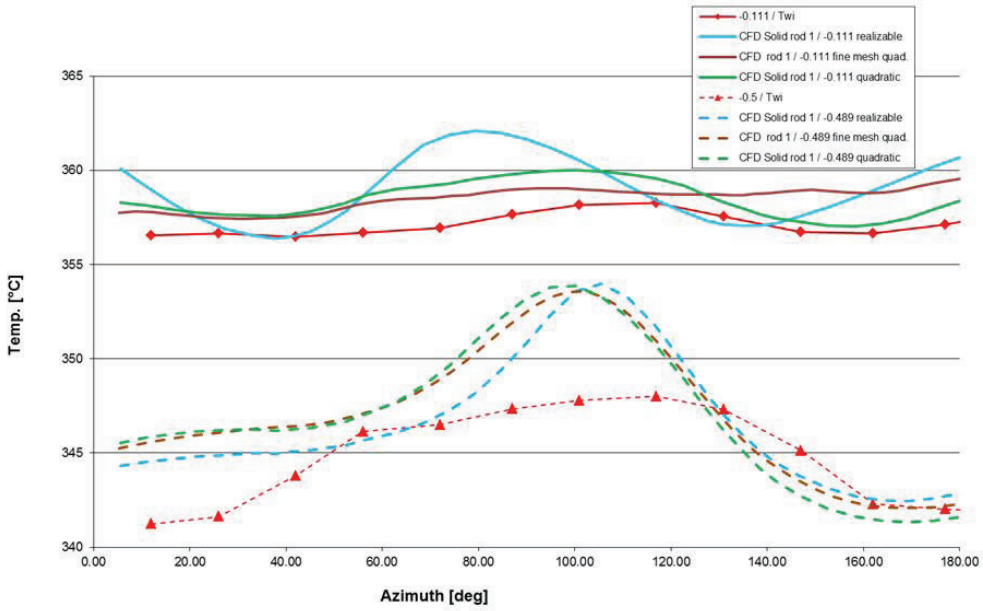

Figure 13: Circumferential inner wall temperature for Rod 1 at two elevations

3.3. Results

Inside wall temperatures were measured during this test using a sliding temperature probe. The apparatus is described in [1]. In order to compare the wall temperature, the inner-wall temperatures are extracted from the CFD results (called Twi). This is why it is crucial to include the conduction throughout the cladding in order to be able to compare the resulting local temperature at the measurement location. This temperature is a function of the local fluid temperature on the other side of the wall as well as the three-dimensional conduction inside the cladding. Temperatures were measured only in the center rods (hot rods). As previously mentioned the measurement technique allowed both an axial and azimuthal resolution. In this paper, two rods are used to illustrate the comparisons: the center rod (rod 5) and the corner rod (rod 1). For each rod the circumferential distribution of the inner-wall temperature is presented at four elevations around the MVG and the SSG. Figure 14 shows the axial and azimuthal orientation while Figure 15 presents a map of the rods and subchannels.
For Rod 5, Figure 16 shows the circumferential temperature distribution upstream of the spacer. Because the flow is fairly uniform, away from the previous spacer, the circumferential fluctuations are fairly weak and considering the uncertainty of the measurements. Figure 17 and Figure 18 show the temperature distribution at two elevations downstream of the spacer grids. Fluctuations are stronger due to the disturbances induced by the MVG. The wall temperature of the location facing the subchannels is cooled versus the locations facing neighboring rods. The azimuthal fluctuations slowly decrease as one goes up in the span. Figure 19 presents the temperature after the SSG. The fluctuations have mostly disappeared, some impact of the spacer is still captured by CFD but barely present in the measurements. It seems that CFD is slightly over-predicting the average wall temperature (seen in Figure 16 and Figure 19). The peaks are also slightly over-predicted by CFD. This could be explained by a measurement deficiency to capture local values since the peaks are extremely localized, it is possible that some averaging is performed by the measuring probe. Additional input would also be needed to take into account the heat losses of the bundle, which were assumed to be zero for the CFD model. CFD prediction and measurements are well in phase. Figure 16 seems to show a misalignment of the temperature distribution but this is probably attributed to the lack of gradients around the rod.

Some results for Rod 1 are also presented. Because of its surrounding Rod 1 presents an interesting unbalance in the flow and the surrounding conditions. Overall the same conclusions apply. The "cold" region is capture by CFD for angle greater than 180 degrees as for the measurements. Upstream of the spacer, Figure 20 shows very little fluctuations. A small drop in temperature is predicted by CFD and shown by the measurements. Downstream of the MVGs, Figure 21 and Figure 22 show the same fluctuations induced by the enhanced cooling provided by the MVG. For angles greater than 180 degrees, the temperature is significantly decreased. This phenomenon is captured by both the CFD and the measurements. Again the CFD prediction seems to slightly over-predict the peaks. Finally downstream of the SSG on Figure 23, most of the fluctuations are removed. The measurements merely show the impact of the flow features, however there is an obvious drop in temperature for angles greater than 180 degrees. CFD predicts the same drop however the temperature remains slightly over-predicted and some effects (proximity of the neighboring rods) are still captured. The CFD seems to follow fairly well the trends induced by local cooling due to the improved cooling provided by the MVG. The peaks are slightly over-predicted compared to the measurements and the overall temperature seems to be slightly higher. It becomes more obvious as the temperature fluctuations become weaker.
A larger number of measurements were performed and compared with the CFD predictions. The conclusions are fairly consistent and overall show a good ability of this model to predict wall temperature and the impact of the flow on the wall along with the enhanced cooling caused by the presence of the MVG. CFD also achieves a good spatial agreement with the measurements. Low azimuthal gradients (far wake regions) are more challenging both to measure and predict. This could explain the slight shift in peaks location between measurements and predictions.

3.4. Fluid temperature

During the same OMEGA experiment, fluid temperatures were measured in each subchannel at the EOHL using a thermocouple rake. This data was also used to compare CFD predictions from a fluid point of view. Typically these measurements are very sensitive as there can be strong temperature differences as one gets closer to the heated walls as illustrated in Figure 24. Accuracy in the location of these measurement probes is key (and difficult to achieve) and can introduce high uncertainty. The reported spatial uncertainty is ±1.5mm which can have a significant impact on the measured temperature. Fluid temperatures are extracted from the CFD at the EOHL and compared with measurements.
Figure 25 shows the difference between the CFD prediction and the measured temperatures at the center of each subchannel. The channel numbering is consistent with the numbering showed in Figure 15. Overall the difference is within 2°C and the CFD seems to slightly over predict the fluid temperature consistently (except for a few peripheral channel). Considering the uncertainty associated with the probe location, this is a satisfying result.

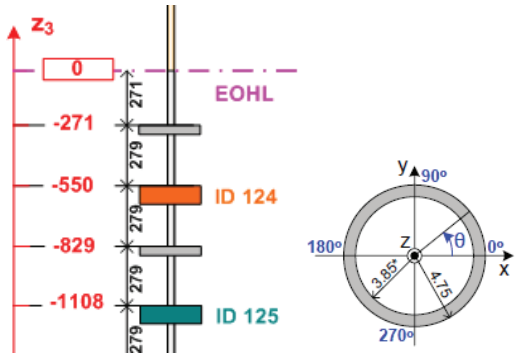

Figure 14: Axial and azimuthal location

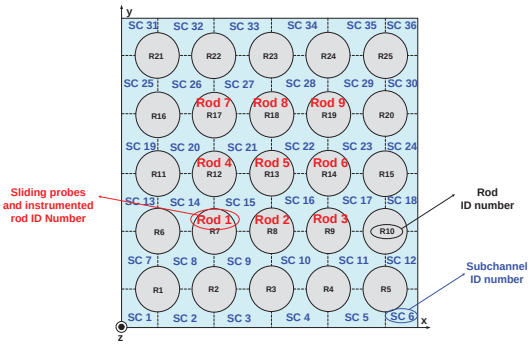

Figure 15: Rods and subchannels map

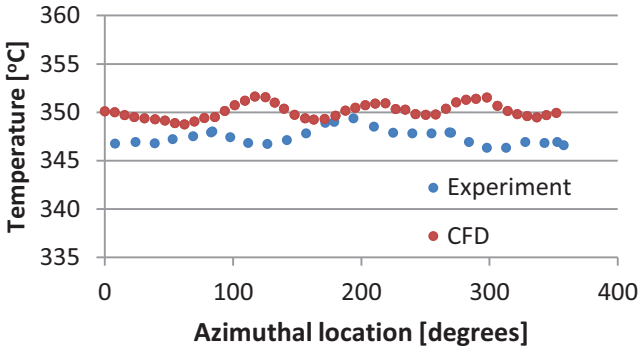

Figure 16: Circumferential inner-wall temperature for Rod 5 at Z_3=-1150mm

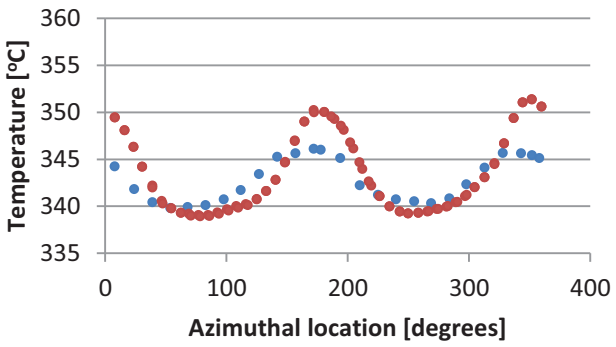

Figure 17: Circumferential inner-wall temperature for Rod 5 at z_3=-1030mm

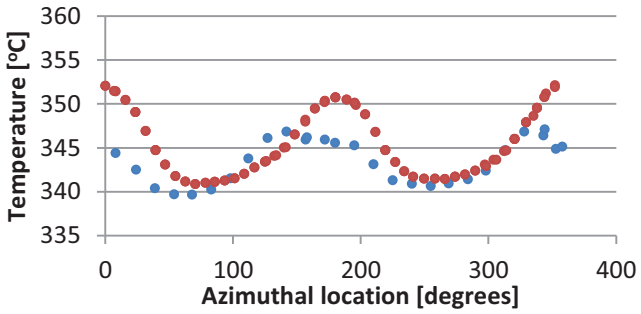

Figure 18: Circumferential inner-wall temperature for Rod 5 at z_3=-1000mm

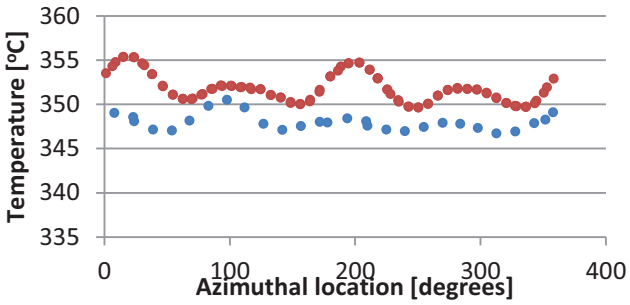

Figure 19: Circumferential inner-wall temperature for Rod 5 at z_3=-790mm

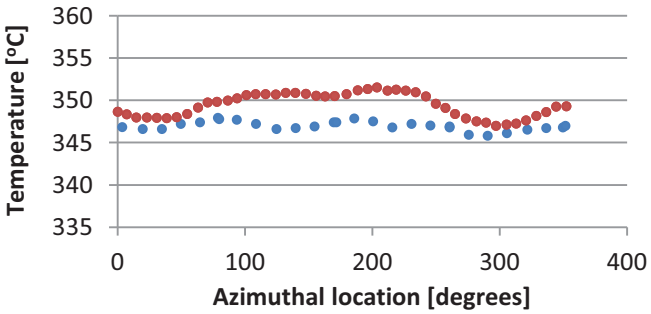

Figure 20: Circumferential inner-wall temperature for Rod 1 at Z_3=-1150mm

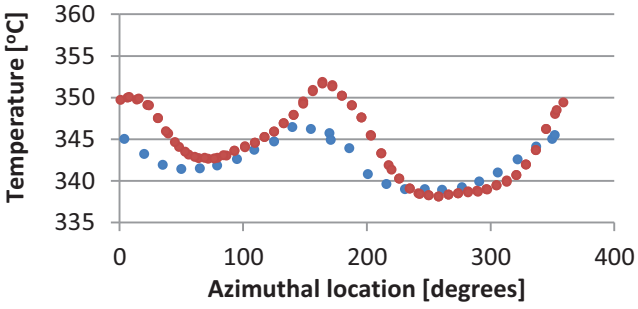

Figure 21: Circumferential inner-wall temperature for Rod 1 at Z_3=-1030mm

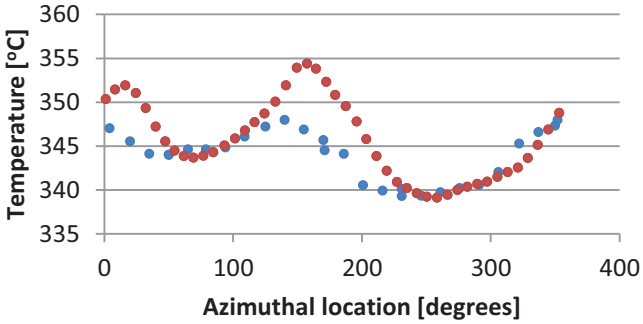

Figure 22: Circumferential inner-wall temperature for Rod 1 at Z_3=-970mm

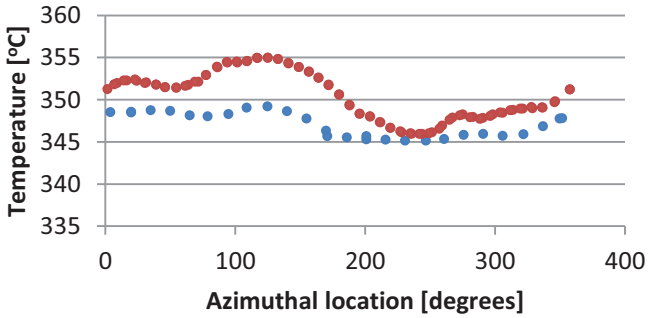

Figure 23: Circumferential inner-wall temperature for Rod 1 at Z_3=-790mm

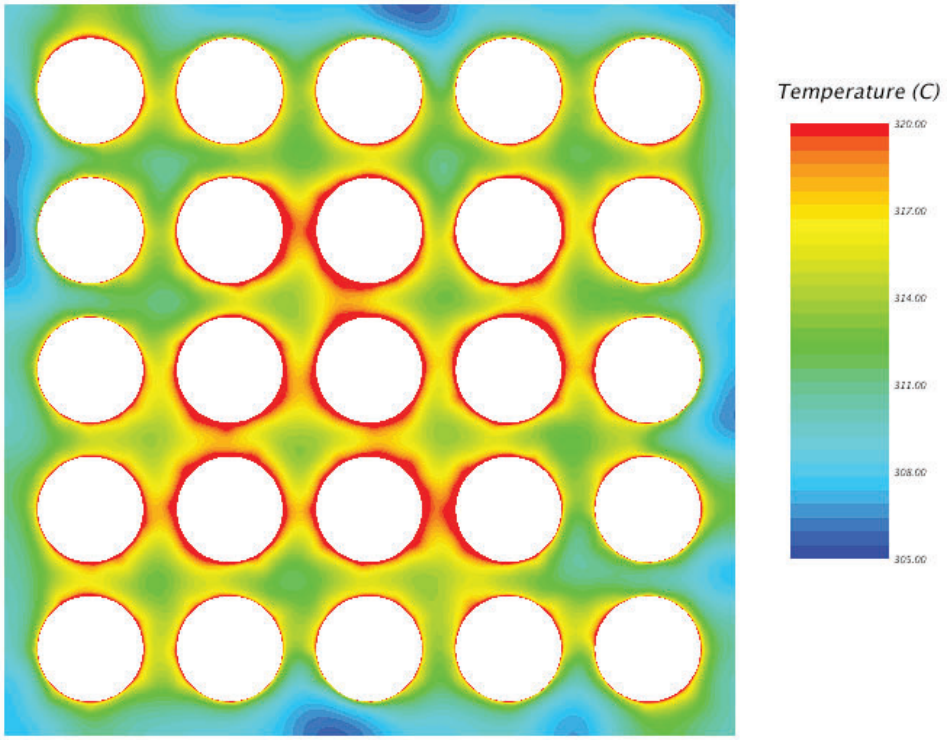

Figure 24: Fluid temperature distribution at the end-of-heated-length.

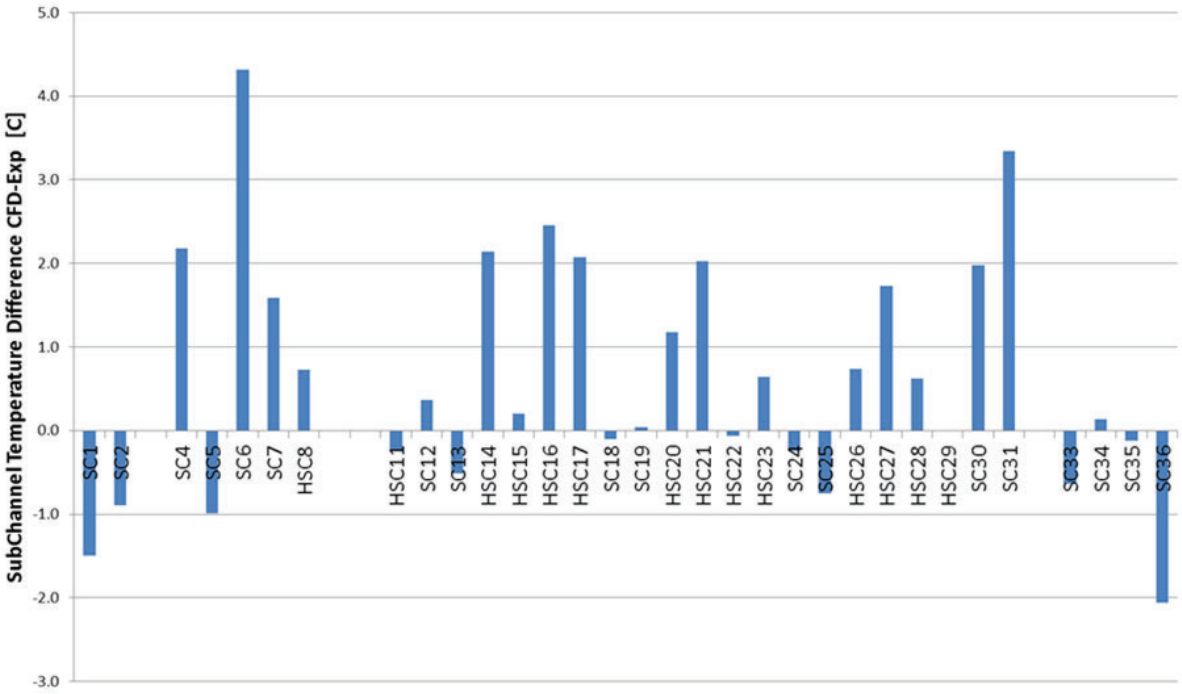

Figure 25: Subchannels temperature difference (CFD – measurements) [^{o}C]

4. CONCLUSIONS

The EPRI Round Robin benchmark allowed participants to benchmark their CFD method to the high fidelity NESTOR data. This paper presents some of the results of AREVA's simulations in this benchmark. It is not possible to present the extent of the comparisons between the CFD model and the experiments but the main conclusions and highlights are presented in this paper.
AREVA's CFD best practices showed good agreement with the measurements. All the critical TH quantities were measured and modeled throughout this benchmark proving the ability of CFD to accurately predict all aspects of the single-phase TH conditions in a fuel bundle. The modeling strategy relying on steady RANS (Reynolds Averaged Navier Stokes) provided a good trade-off between accuracy and computational cost for this particular application.
This benchmark also highlighted the necessity of understanding the conditions and test set up, in order to accurately model the experiment and the measurement conditions. CFD is a very precise and detailed tool and the challenge is to properly include all the contributing aspects in the model, for example the necessity of modeling the cladding to properly resolve wall heat flux, hence wall temperature.
The good agreement achieved in this benchmark against representative TH measurements in fuel assemblies confirms that CFD is capable of providing accurate and reliable TH quantities for level IV Crud risk assessment.

ACKNOWLEDGMENTS

The authors of this paper would like to thank EPRI, CEA, EDF and Texas A&M for organizing this benchmark and allowing participants to access this high fidelity NESTOR data. The other participants of the benchmark should also be acknowledged since the work presented here is also the result of a collaborative effort as far as modeling techniques and discussions about the phenomena at stake in these challenging conditions.

REFERENCES

1. A. Bergeron, T. Chataing, E. Décossin, J. Garnier, P. Péturaud, S. K. Yagnik, "Design, Feasibility, and Testing of Instrumented Rod Bundles to Improve Heat Transfer Knowledge in PWR Fuel assemblies", *Proceedings of the 2007 International LWR Fuel Performance Meeting,* San Francisco, California, (2007)
2. P. Péturaud, S. K. Yagnik , "Overview of CFD Round Robin Benchmark of the High Fidelity Fuel Rod Bundle NESTOR Experimental Data", *Proceedings of NURETH 16*, September 2015
3. J. H. Jones, M. G. Martin, T. H. Keheley, R. L. Harne, M. G. Pop, C. C. Lascar, J. Simoneau," AREVAs Comparative Process for CILC Risk Assessment Using Subchannel and CFD Modeling", *Proceedings of LWR Fuel Performance Meeting, Top Fuel, WRFPM,* Orlando Florida, (2010).
4. C. Lascar, M. Pierre, K. Goodheart, M. Martin, A. Hatman and J. Simoneau, "Validation of a CFD Methodology to Predict Flow Fields within Rod Bundles with Spacer Grids", *Proceedings of NURETH 15-069*, Pisa, Italy, May 2013
5. CD-adapco™, Inc., "User Guide – STAR-CCM+® Version 8.06," 2013.
6. E. Baglietto, H. Ninokata, T. Misawa, "CFD and DNS Methodologies Development for Fuel Bundle Simulations," *Nuclear Engineering and Design*, **Vol. 236**, pp. 1503-1510, (2006).